Finite Element Simulations of Motorcyclist Interaction with a Novel Passive Safety Concept for Motorcycles

Steffen Maier, Laurent Doléac, Holger Hertneck, Sebastian Stahlschmidt, Jörg Fehr

Abstract Motorcycle accident scenarios are inherently complex and unpredictable. In severe accidents, motorcyclists often suffer multiple serious injuries. Would it be safer for a motorcycle rider to be restrained to the motorcycle rather than exposed to the unpredictable sequence of the accident? What methods allow us to answer this efficiently for the many possible scenarios? To investigate those research questions, a motorcycle model and a novel safety concept, a combination of thigh belts, airbags, and impact protectors, were developed in a finite element simulation environment for detailed rider-to-motorcycle interaction. Restrained surrogate models of a small female and mid-sized male rider were studied in various impact configurations.

Restraining the rider to the motorcycle, decelerating the resulting upper-body motion with airbags and the interaction of upper and lower extremities with the handlebar and leg impact protectors led to a guided and controlled trajectory. The methodology used as part of a multi-stage development process, with increasing complexity and expected fidelity, allowed detailed representation of diverse motorcyclists and their interaction with a motorcycle while efficiently incorporating full vehicle interaction.

Keywords Motorcycle Safety, Motorcycle-to-Car Collisions, Finite Element Simulations, Passive Safety, Vulnerable Road Users.

I. INTRODUCTION

Motorcyclists currently have a disproportionate risk in road traffic. In 2015, motorcyclist fatalities accounted for 15% and moped rider fatalities accounted for 3% of all traffic fatalities in Europe [1]. In 2019, in Germany, e.g., the number of fatalities measured by motorcycle registrations was five times higher than for passenger cars [2]. Measured by the total mileage of 10 billion kilometres of motorcycles compared to 632 billion kilometres of passenger cars, the number of fatalities was 25 times higher [2-3]. The reason for this high susceptibility to injury is the insufficient passive protection of riders on motorized two-wheelers.

A recent analysis of 40 serious urban accidents of powered two-wheelers, mostly scooters, with other vehicles [4] showed that the main crash configurations were head-on collisions of a motorcycle impacting into a car's side (45%), front (20%) and rear (10%), followed by sideswipe collisions (15%) and side impact by cars (7.5%). Overall, in 75% of the accidents surveyed the motorcycle's impact was at its front, while a further 22.5% was at its sides. Injury analysis showed that serious injuries with MAIS3+, according to the Maximum Abbreviated Injury Scale (MAIS), occurred at thorax (70%), head (40%), lower limbs (37.5%), abdomen (20%) and spine (2.5%). The in-depth study concluded that in the accidents surveyed, the thorax requires more protection, followed by the head – despite the fact that a helmet was worn in all cases – and the lower limbs. A recent study on traffic-related fatalities [5] also reported that out of the 570 motorcyclist fatalities surveyed, and their passengers, 63.7% died because of multiple injuries. These injury data sets indicate that the high mortality rate is not related to single critical body regions. Therefore, reducing severe injuries and fatalities requires the protection of the whole body. For conventional motorcycles, it is considered advantageous that the rider separates from the motorcycle as soon as possible and does not become entangled in parts of the motorcycle body [6]. In conjunction with the current most frequently used personal protective equipment, such as safety clothing and helmets, as the data have shown, adequate protection is not given to a motorcyclist's entire body. This leads to our central research questions: is it safer for a motorcyclist to be restrained to the motorcycle

S. Maier (e-mail: steffen.maier@itm.uni-stuttgart.de; tel: +49 711 685-66956) is a research associate and doctoral student and J. Fehr is Professor at the Institute of Engineering and Computational Mechanics (ITM) at the University of Stuttgart, Germany. L. Doléac is the founder of Doléac Models, Ostfildern, Germany. H. Hertneck is director of sales and development at SAS-TEC GmbH, Markgroeningen, Germany. S. Stahlschmidt is head of the competence field dummy models at DYNAmore GmbH, Stuttgart, Germany.

rather than exposed to the unpredictable sequence of the accident? What research methods allow us to answer this efficiently and effectively for the many possible accident configurations?

Current efforts to protect motorcycle riders include (i) personal protective equipment, such as safety clothing, helmets, neck braces and wearable airbag devices, (ii) airbags mounted to the motorcycle, e.g., [7], and (iii) enveloping structures, e.g., [8]. In the past, there have been few efforts to restrain a rider to a two-wheeler. In [9], a safety jacket was investigated, which was connected to the rear of a motorcycle with a single belt at the back. In simulations it was shown that it is possible to reduce head and neck loads in a collision between a motorcycle and a moving car by preventing the head from hitting the car. Murri [10] investigated a similar harness consisting of shoulder, lap, and crotch straps for a motorcycle rider in crash tests to prevent contact between the rider's head and the collision opponent. To date, the BMW C1 scooter remains the only sold two-wheeler to feature seat belts [8]. The rider is strapped to the vehicle in an upright position with two seat belts that run diagonally across the chest. In combination with the safety cell, it offers a high degree of passive protection and is therefore exempt from the legal helmet requirement in many European countries.

Studies on motorcycle crash safety, especially in crash simulation, are not at all on a par with passenger car crash safety. Nevertheless, new virtual methods are needed to simulate motorcycle accidents at different levels of detail and system complexity. To answer the research questions, what is needed is a model with detailed rider-to-motorcycle interaction and simulation methods that incorporate accident dynamics of collisions with cars. For the conceptual studies with many accident scenarios, this model must be numerically efficient. Based on a new safety concept for motorcycles, where the motorcyclist is restrained to the motorcycle, such a model, with a level of detail and model complexity between a MB simulation model and a FE simulation representing full vehicle interaction, was investigated in this work. Within the given process it is shown: (i) how to position FE dummy models on a motorcycle; (ii) how to transfer accident motions from a MB to FE analysis; and (iii) how to include a foam material. The novelty of the presented work is a detailed FE model of the novel safety concept, i.e. restraining the rider, which accurately predicts and evaluates the rider-to-motorcycle interaction. This novel approach to understanding motorcyclists' guided accidents kinematics is the first step towards a reproducible rating of injury mitigation systems for motorcyclists, of the kind currently established only in occupant simulations in cars.

II. METHODS

To capture an environment with many design variables and parameters, a multi-stage development process was applied with approximation stages through simulations and with successive increases in complexity and expected fidelity. The first step was to model the motorcycle with safety concept in a combined MB and FE approach in the MADYMO software environment [11], which allowed many simulations to test and fine-tune the system. In the stage presented here, a detailed FE model of the novel safety concept was developed for accurate rider-to-motorcycle interaction in LS-DYNA (version LS-DYNA R9.2.0), to verify the results and increase the level of detail. As set out in the description that follows, the trajectories from the MB simulation were used to represent the accident motion in the FE simulation. Numerical rider surrogate models, a 5th and a 50th percentile Hybrid III dummy (LSTC Detailed release 190217) representing a small female and a mid-sized male rider, were positioned onto the motorcycle to capture the rider's interaction with the motorcycle and its passive safety systems for multiple impact configurations. To improve the lower extremities' protection, i.e. the legs, an energy absorbing foam material was experimentally tested and numerically characterized.

Multi-Body Trajectory Implementation

To replicate the crash dynamics of the motorcycle in accidents, the motorcycle was modelled as a MB model with three rigid bodies in a previous work [9]. These bodies, the body of the motorcycle and its wheels, were coupled to replicate (i) rotating wheels, (ii) front and rear suspension, (iii) front fork steering, and (iv) front fork impact deformation. The model parameters of the motorcycle and the accident opponent, a passenger car, were based on fitted simulation models of full-scale crash tests of conventional motorcycles and Hybrid III 50th percentile dummies in sitting configuration colliding with cars from Dekra [6] in two of the seven shown accident scenarios. To describe the accident dynamics of the motorcycle and car in the work presented here, rigid body trajectories from these MB simulations of the motorcycle and car were used, as shown in Fig. 1. The outer body geometry of the motorcycle and the car's body geometry were implemented as imposed motions by their initial linear

velocities with linear acceleration and angular velocity time histories of the rigid bodies in the MB environment. This procedure corresponds to simulations or experiments of vehicle occupants in which the accident interaction with an accident opponent is also substituted by motion profiles of the car interior. Here, the rigid body trajectory is described by a multi-axial movement of motorcycle and car. The car's body geometry acts solely as reaction surfaces for the airbags.

Based on the MB simulations, the motorcycle and riders were simulated in seven representative accident scenarios for motorcycles colliding with passenger cars in an initial upright motorcycle position, according to ISO 13232-2:2005 [12], which describes very frequent accident scenarios based on 501 real motorcycle-to-car accidents in Hannover, Germany, and Los Angeles, USA. The set does not include collisions with roadside barriers and the evaluation is limited to the primary impact, the immediate period after contact of the two vehicles.

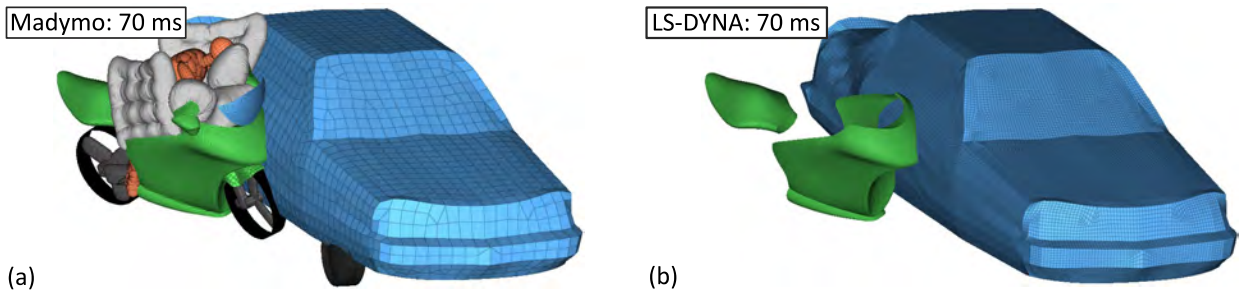

Fig. 1. (a) Simulation of dummy and motorcycle with passive safety equipment against opponent car in Madymo MB simulation environment. (b) Accident kinematics of prescribed rigid outer body of motorcycle and prescribed rigid body of car with finer discretization in LS-DYNA FE simulation environment.

Motorcycle Cockpit with Passive Safety Components

The rider interaction surfaces are depicted in Fig. 2. The inner cockpit, attached to the prescribed rigid outer body, was modelled as a very stiff 2D shell surface representing 2 mm sheet steel. The receding windshield fails under front airbag pressure to allow more forward displacement of the rider in case of airbag deployment and was modelled as a 2D shell representing 4 mm plastic material. The handlebars with hand grips, the footrests, and the rear-view mirrors are approximated as rigid body shells, fixed to the prescribed outer body.

The concept's passive safety components, consist of two thigh belts, five airbags and two leg impact protectors. The airbags were modelled with identical geometry to the initially scaled and undeformed 2D reference mesh of the Madymo model [11], with equivalent deployment using the uniform pressure technique, with an ideal gas formulation and an adiabatic process. The belts were represented by significantly finer discretized 2D mesh and 1D beam elements with combined belt pretensioning and load-limiting and similar operating mode to the Madymo implementation. After detection of an accident the belts are pretensioned until a force limit is reached. During the accident, this force limit is further applied by increasing belt length to provide a constant force level. The design variables of the airbags, the mass inflow and the outflow area, and the belts, the belt pay-in function and belt load limit, and the ambient state variables were kept identical to the Madymo model.

The foam impact protectors were modelled using 3D solid elements. The protectors have a constant thickness of 15 mm and are flush with the adjacent motorcycle cockpit surface, surrounding the rider's thighs and knees. The protectors are intended to provide a soft surface and must achieve good impact energy absorption. The

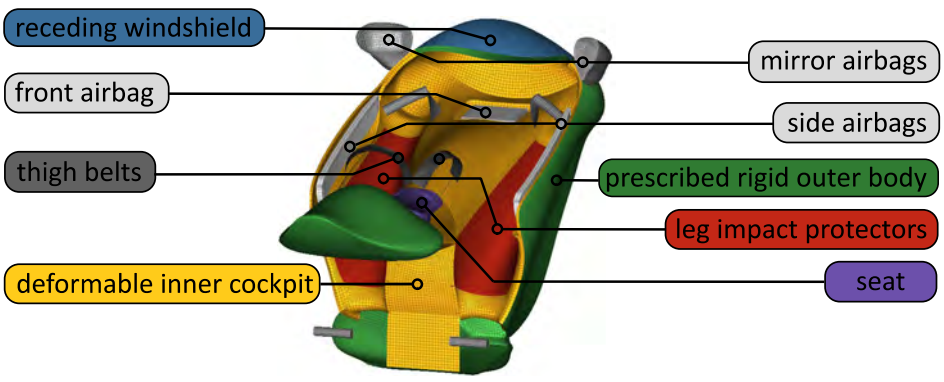

Fig. 2. Components of motorcycle's cockpit with passive safety concept.

designated protector material, an energy absorbing foam, can be produced in different densities and has an impact-rate-dependent material behaviour. On fast impacts, it is very firm, while under slower loading it remains soft. In the current applications it proves effective. It is used e.g. in commercially available shoulder, knee, elbow and back protectors that are worn, among others, by riders of powered and non-powered two-wheelers or horses. To numerically model this behaviour in LS-DYNA, the material model **MAT_FU_CHANG_FOAM* is well suited and was chosen. The material model reproduces rate-dependent loading and hysteretic unloading of low and medium density foams, has a variety of useful material behaviour calibration functions, and is designed for near-test conditioning [13]. For the required stress-strain curves of the material model, several strain rates dynamic tests with a pendulum impactor (see Fig. 3) and quasi-static tests with a universal testing machine were conducted. Five measurements each, shown in Fig. 4, were made for four dynamic and one constant loading.

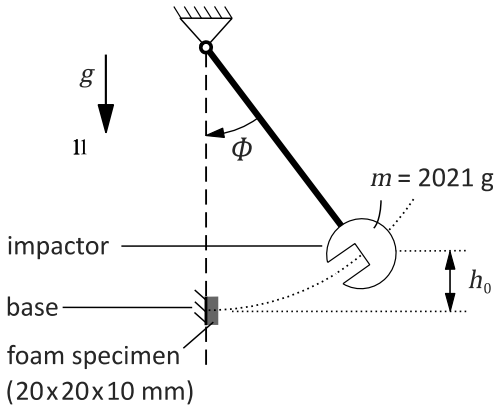

Fig. 3. Schematic of the dynamic pendulum, with flat impactor surface and mass m, dropped from height h_0 on foam specimen with force sensing in rigid base and displacement measurement via pendulum angle Φ.

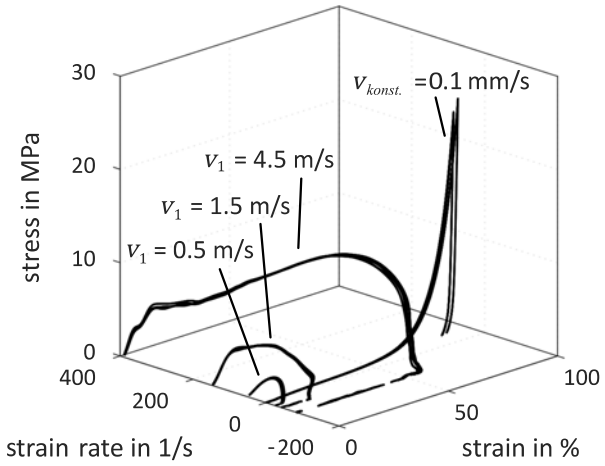

Fig. 4. Stress-strain-strain rate data from experiments with dynamic impact velocities v_1 of 0.5 to 4.5 m/s and constant velocity $v_{konst.}$ of 0.1 mm/s for foam density of 425 g/l. Note: measurement $v_{konst.}$ cuts off after the specimen detaches from the impactor due to the very slow unloading response of the foam samples.

The LS-DYNA **MAT_FU_CHANG_FOAM* material card requires strain-stress curves with constant strain rates. The dynamic loading test data with impact velocities v_1 of 0.5 to 4.5 m/s were fitted up to their maximum stress using bipolynomial regression on a rectilinear grid as shown in Fig. 5. The curves for the material card, which describe the rate-dependent loading behaviour, then correspond to cross sections of this surface. To determine the unloading behaviour the quasi-static unloading test data with the constant impact velocity $v_{konst.}$ of 0.1 mm was fitted using a polynomial fit, also shown in Fig. 5. Detailed information of the applied surface fit using bipolynomial regression through minimization of a quadratic objective function are provided in Appendix A.

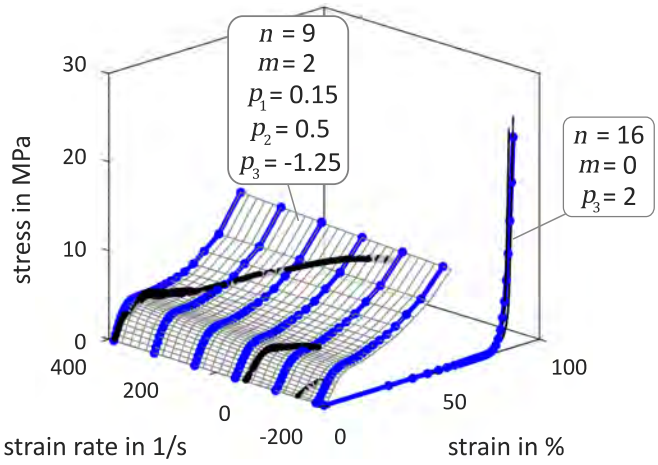

Fig. 5. Polynomial material card curves (blue) fitted to loading data of dynamic experiments and unloading data of quasi-static experimental data with respective parameter choice of surface fit. See Appendix A for parameter determination.

In the material model, the hysteretic unloading behaviour is then determined through the curve with the lowest strain rate, with damage formulation d for the principal stresses σ_i:

$$\sigma_i = (1-d)\,\sigma_i \qquad \text{with} \qquad d = (1-\mathrm{HU})\left[1-\left(\frac{W_{current}}{W_{maximal}}\right)^{\mathrm{SHAPE}}\right]^{\mathrm{EXPON}}, \tag{5}$$

where W is the hyperelastic energy, $\mathrm{HU} \in [0,1]$ is a hysteretic unloading factor, and SHAPE and EXPON are a shape factor and exponent for unloading, respectively [13]. To review the choice of HU, SHAPE and EXPON and to verify accurate simulation for impactors smaller than the foam specimens and with different geometries, tests with varying impactor geometries, masses and drop heights were conducted with a drop tower impactor, as schematically shown in Fig. 6. As the results show, the force responses of the simulations conform well to the experiments both in magnitude and in shape.

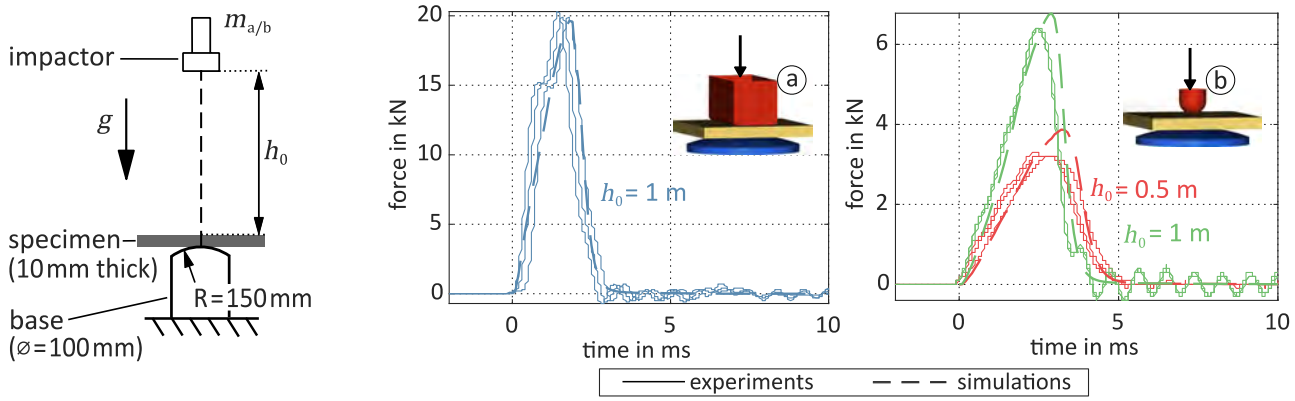

Fig. 6. Schematic of impactor drop tower setup with drop height h_0 on foam specimen with force sensing in rigid base. Comparison of force sensor response of experiments with simulations for configurations of impactor ⓐ (m_a =5031 g, width = 80 mm, depth = 40 mm) and ⓑ (m_b = 2404 g, radius = 12.5 mm) and foam density of 425 g/l.

Male and Female Motorcycle Rider Surrogates

The norm ISO 13232-3:2005 [12], which specifies methods and procedures for the assessment of motorcycle protection devices, recommends the use of the motorcyclist anthropometric test device (MATD), a modified version of a 50th percentile Hybrid III in frontal configuration for all impact scenarios. These modifications are (i) a modified neck and head compatible with motorcycle helmets in motorcycle-specific head positions, (ii) a sit/stand pelvis and (iii) frangible components in the abdomen, upper and lower legs, and knees. Despite the recommendation and concordant with [11], numerical representations of the Hybrid III dummy family were used. The reasons were that (i) the MATD has significant clefts at the hip attachment points not suited to fasten thigh belts, (ii) no helmet is used and helmet compatibility is no therefore no requirement, (iii) the MATD dummy is not available as a FE model in LS-DYNA, and (iv) we want to assess a diverse group of riders with 5th percentile surrogate representing a small female rider and the 50th percentile, representing a mid-sized male rider.

The positioning of a Hybrid III dummy, initially designed as a surrogate for occupants of frontal crash scenarios, into the postures of motorcyclists led to some difficulties. The prepositioning tools for FE dummies using node displacements based on the kinematic joints of the dummy are very limited. For great variations in the posture, overlapping elements can occur. Here, for the Hybrid III family, this occurred for some locations, particularly: (i) the thighs-to-pelvis connections of the moulded hip flexion angle, (ii) the knee bends, where the shanks touch the thighs; and (iii) the dummy wrists. To avoid overlapping, methods that incorporate compliance between deformable parts in transient simulations were applied. In a first step, an initial posture, which was as close as possible to the desired posture, was achieved using the above-mentioned nodal displacements constrained solely by the kinematic dummy joints. Subsequently, simulations were performed to examine self-contacts, where the dummies were partially locked and constrained by elastic elements to prescribed motion nodes, as schematically shown in Fig. 7 for the 50th dummy. Initially, scaled and distorted geometries of the contact partners were implemented that move to the final motorcycle geometry. This was used to rotate the wrists, spread the legs, bend the knees, raise the head, and initialize contacts with the handles, footrests, seat, belts and cockpit surface,

to the final postures depicted in Fig. 8.

The actual accident simulations start immediately before impact with the rider in the prepositioned seated state. During the accident, contact of the dummy with the motorcycle parts with the passive safety components shown in Figure 2 were considered. Contacts of the dummy's head, upper torso and upper extremities with the accident opponent, the car, were avoided by the safety concept. Contacts of the lower extremities with the car were neglected since the cars motion is predefined and thus the undeformable car geometry pierces trough the motorcycle's side impact structure. In the following this concerns scenarios with significant lateral motorcycle to car interaction.

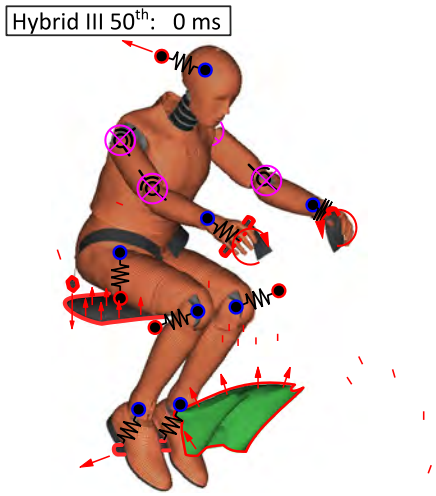

Fig. 7. Initial posture and representation of prepositioning methodology exemplary for 50th Hybrid III with prescribed motion nodes (red), elastic coupled dummy nodes (blue) and locked joints (magenta).

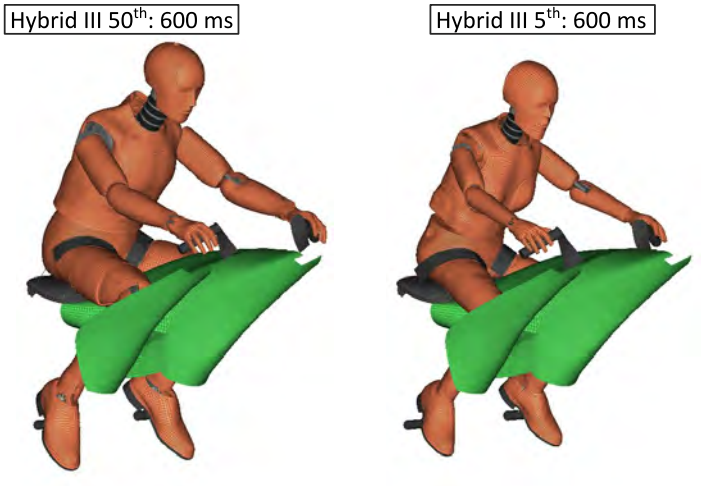

Fig. 8. Final seating posture, with contact initialization of 5th and 50th Hybrid III with motorcycle cockpit, seat and belts in the final state of the prepositioning simulation.

III. RESULTS

In the seven representative accident scenarios recommended by ISO 13232, the motorcycle impacts into or gets impacted by a passenger car at various relative speeds and relative angles. The norm's nomenclature XXX – YY/ZZ of the impact configurations consists of a three-digit code for the relative geometric positions of the motorcycle and opposing vehicle at impact (XXX), the speeds at impact in metres per second of the opponent vehicle (YY) and motorcycle (ZZ).

For all the accident configurations shown in Fig. 9, the accident kinematics of the female and male rider surrogates were influenced by the safety system in a similar way. The belts restrained the rider to the motorcycle, with the belt load-limiting devices limiting the pelvis accelerations. The belts established a pivot point to guide the upper body in forward and sideward rotations and kept the riders' bodies within the range of the airbags, leg protectors and side-impact protection structure. The airbags surrounded the riders and decelerated the upper-body trajectory pivoting around the belt restrain. They protected the head and thorax from contact with hard surfaces, such as the uncushioned motorcycle cockpit surfaces and the accident opponent. In this way, the motorcycle itself and the accident opponent acted as reaction surfaces for the airbags.

As shown in the quantitative overview in Fig. 10, the observed critical loads were the head, thorax and pelvis accelerations and neck tensile forces in impact scenarios in which the motorcycle and passenger car are in 90° relative angle. These loads were safety concept-related, mainly dependent on the implemented belt load limit, which is a trade-off between tolerable body loads and feasible body displacement within the passive safety equipment range. Lower belt load limits would reduce above-mentioned head, neck, thorax and pelvis body loads, but would also increase the elongated belt lengths and therefore the risk of the head hitting the accident opponent and reducing the effective restraint of the rider in the subsequent secondary impact phase. As indicated by high loads for upper and lower legs, the leg protectors were important in the lateral impact cases. With a very low profile of only 15 mm, the leg protectors still reduced the impact forces and kept the loads of the upper extremities within the recommended biomechanical limits, while still exceeding the criterion for lower legs in some configurations. A comparison of the loads of the female and male rider surrogates indicates lower loads

relative to the biomechanical limits on the 5th Hybrid III when assuming the same limits.

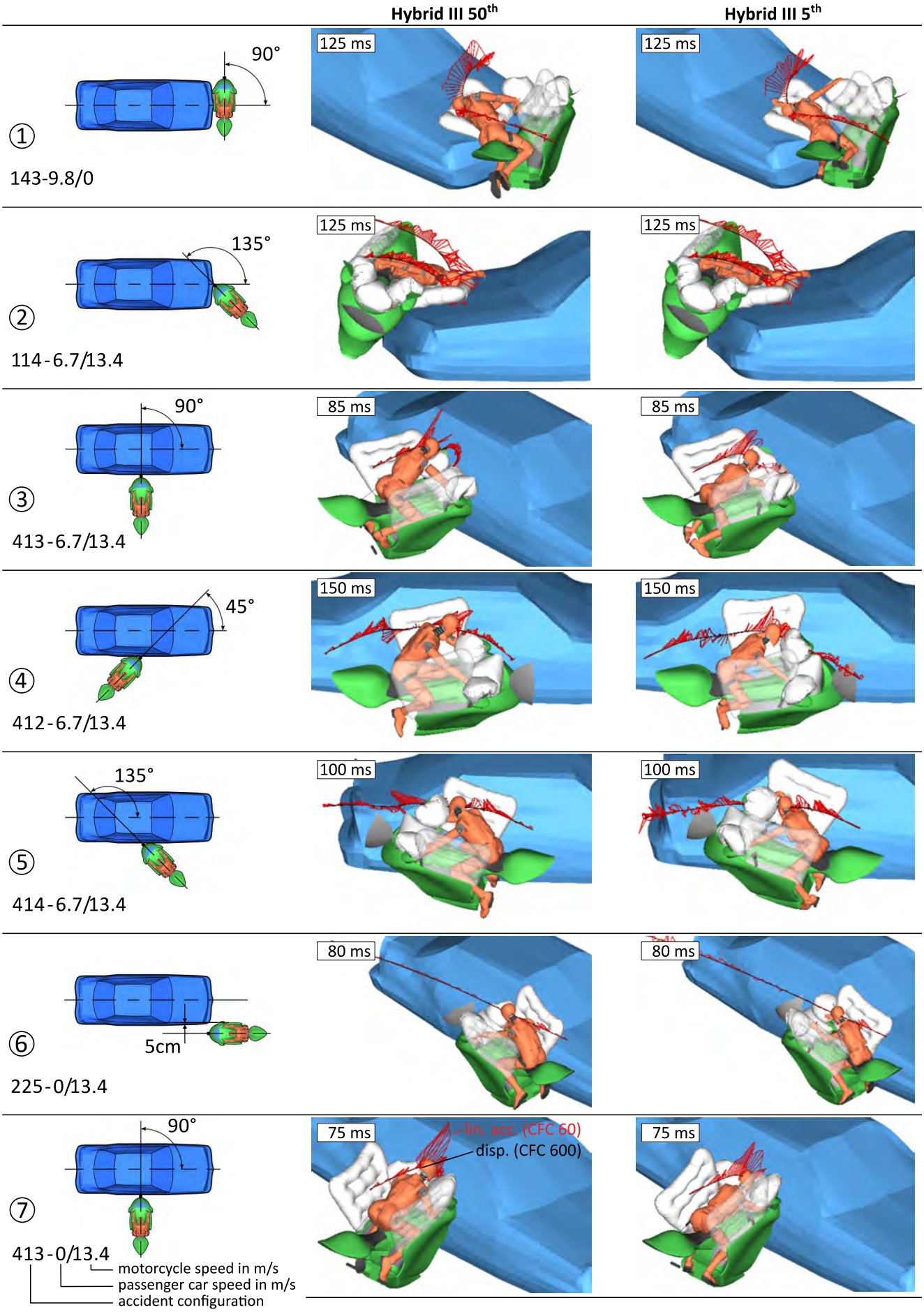

Fig. 9. Simulations of 50th (left) and 5th (right) Hybrid III in all ISO 13232 configurations, with head displacement

trajectory and resultant linear acceleration relative to the reference space for the primary impact up to 0.3 s.

Injury Criteria Relative to Biomechanical Limits for Male and Female Dummy

To quantitively correlate the simulated body loads and potential human rider injuries, a set of injury criteria and respective biomechanical limits from [6], in addition to the neck injury criterion NIJ [14], was used (see Appendix C). The evaluation routine and criteria set from [11] was supplemented by the tibia index (TI), an injury criterion for lower leg loading, which is calculated as the sum of the resultant bending moment (M_{Res}) of the tibia related to a critical bending moment ($(M_{Crit})_{Res}$ = 225 Nm) and the ratio between the axial force (F_Z = 35,9 kN) and a critical axial force ($(F_{Crit})_{Res}$). A limit of 1.3 correlates with a 10% risk of fracture [6].

$$\mathrm{TI} = \left|\frac{M_{Res}}{(M_{Crit})_{Res}}\right| + \left|\frac{F_Z}{(F_{Crit})_{Res}}\right| \leq 1.3 \tag{6}$$

Fig. 10 gives an overview of the chosen set of injury criteria for the 5th and 50th dummies normalized to their respective biomechanical limits and colour-coded to indicate the severity of the body loads. Exemplary for configuration ⑦, the body loads and the derivation of the respective injury criteria are provided in Appendix C.

Hyb III 50th / 5th	head		neck										thorax		pelvis	femur	tibia
	HIC(36)	3ms	z, tens, 1ms	z, tens, 45ms	z, compr, 1ms	z, compr, 45ms	xy, 1ms	xy, 45ms	v, rwd, max	v, fwd, max	Nij_{max}	3ms	Defl max	3ms	$\lvert F \rvert_{max}$		
①	0.27 / 0.31	0.54 / 0.6	0.55 / 0.42	0.76 / 0.27	0.07 / 0.04	0 / 0	0.26 / 0.19	0.37 / 0.19	0.54 / 0.24	0.11 / 0.06	0.34 / 0.24	0.33 / 0.33	0.05 / 0	0.85 / 0.97	0.66 / 0.25	1.59 / 1.05	
②	0.06 / 0.18	0.31 / 0.53	0.3 / 0.23	0.38 / 0.12	0.19 / 0.05	0 / 0	0.14 / 0.09	0.29 / 0.06	0.52 / 0.2	0.08 / 0.08	0.24 / 0.17	0.31 / 0.36	0.14 / 0.07	0.68 / 0.58	0.39 / 0.18	1.45 / 0.32	
③	0.26 / 0.17	0.79 / 0.42	0.73 / 0.34	0.15 / 0.08	0.1 / 0.07	0 / 0	0.35 / 0.21	0.08 / 0.19	0 / 0.17	0 / 0.01	0.39 / 0.18	0.85 / 0.55	0.34 / 0.18	0.93 / 0.63	0.75 / 0.22	0.94 / 0.53	
④	0.16 / 0.18	0.44 / 0.43	0.43 / 0.25	0.14 / 0.11	0.05 / 0.28	0 / 0	0.28 / 0.14	0.38 / 0.17	0.29 / 0.28	0.16 / 0.02	0.29 / 0.2	0.32 / 0.31	0.14 / 0.07	0.65 / 0.84	0.37 / 0.38	0.66 / 0.41	
⑤	0.06 / 0.09	0.34 / 0.43	0.38 / 0.19	0.24 / 0	0.03 / 0.26	0 / 0	0.25 / 0.12	0.38 / 0.1	0.57 / 0.13	0.17 / 0.02	0.29 / 0.18	0.34 / 0.31	0.16 / 0.07	0.77 / 0.62	0.57 / 0.35	0.77 / 0.25	
⑥	0 / 0	0.13 / 0.13	0.13 / 0.13	0 / 0	0.12 / 0.11	0 / 0	0.06 / 0.05	0.09 / 0.07	0.02 / 0.01	0 / 0	0.08 / 0.08	0.1 / 0.14	0.04 / 0.03	0.21 / 0.32	0.04 / 0.04	0.19 / 0.08	
⑦	0.21 / 0.27	0.7 / 0.6	0.82 / 0.41	0.47 / 0.44	0.05 / 0.04	0 / 0	0.34 / 0.12	0.06 / 0.03	0 / 0.03	0 / 0.01	0.44 / 0.22	0.59 / 0.62	0.25 / 0.2	0.87 / 0.7	0.17 / 0.21	0.51 / 0.52	

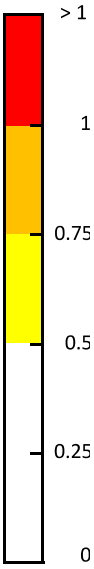

Fig. 10. Injury criteria relative to respective biomechanical limits (Table C.I, Appendix C) for 5th (small female) and 50th (mid-sized male) rider surrogate in all ISO 13232 configurations. Values for the primary impact phase are set to 0.3 s.

Energy balance of the rider's interaction with the passive safety components

To decelerate the motorcycle rider, the rider's kinetic energy must be dissipated through the application of forces. Anything that applies these forces, in this case the airbags, the belts, the impact protectors and the remaining cockpit surfaces, can be considered part of the restraint system. To evaluate the crash energy management of the proposed restraint and its individual contribution, the energy balance of the rider was investigated. Here, the balance of the rider subsystems energies E in LS-DYNA is:

$$E_{total} = E_{kinetic} + E_{internal} + E_{potential} + E_{contact} + E_{sliding\ interface} + E_{hourglass}. \tag{6}$$

The kinetic, internal and potential energies represent the current dummy energy level. The contact energy describes the energy transfer of the dummy contacts with external contact partners. The sliding interface energy is the stored energy of the internal dummy contacts. The hourglass energy is a LS-DYNA-specific numerical quantity and should be comparably low. For impact configurations ① and ⑦ with the 50th dummy, the energy balances are given in Fig. 11. These differ in the rider's initial kinetic energy. In ⑦ the rider's initial velocity is entirely represented by its initial kinetic energy, while in ① the initial velocity, and therefore kinetic energy, is zero. The sign of the accumulated contact energies thus indicates whether energies are absorbed or emitted via the contacts of the rider, and thus determines the combined energy level of the internal, kinetic and potential

energy of the dummy.

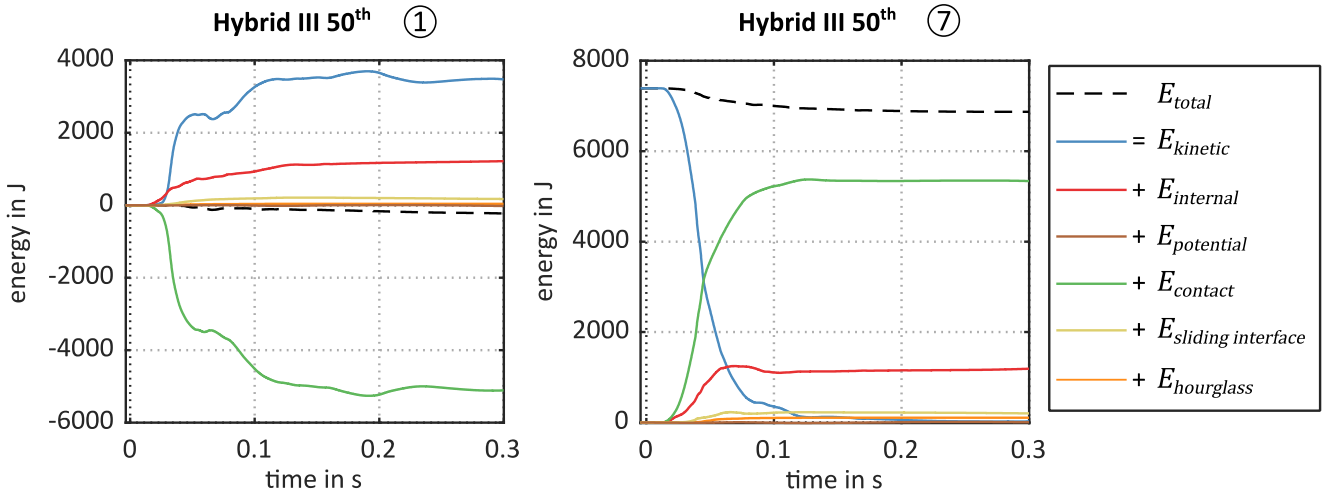

Fig. 11. Energy balance for scenario ① (left) and ⑦ (right) for 50th Hybrid III.

To evaluate the energy balances of all crash configurations with the female and male rider surrogates, Fig. 12 gives the remaining energy portions of the simulations' final state at 0.3 s. To illustrate the distribution of the contact energy transfer, the contact energy is split for its contributing contact partners. Configurations ①, for 5th and 50th, respectively, has no initial kinetic energy. Configurations ② to ⑦ have all the same initial kinetic energy, with an initial velocity of 13.4 m/s or 48 km/h.

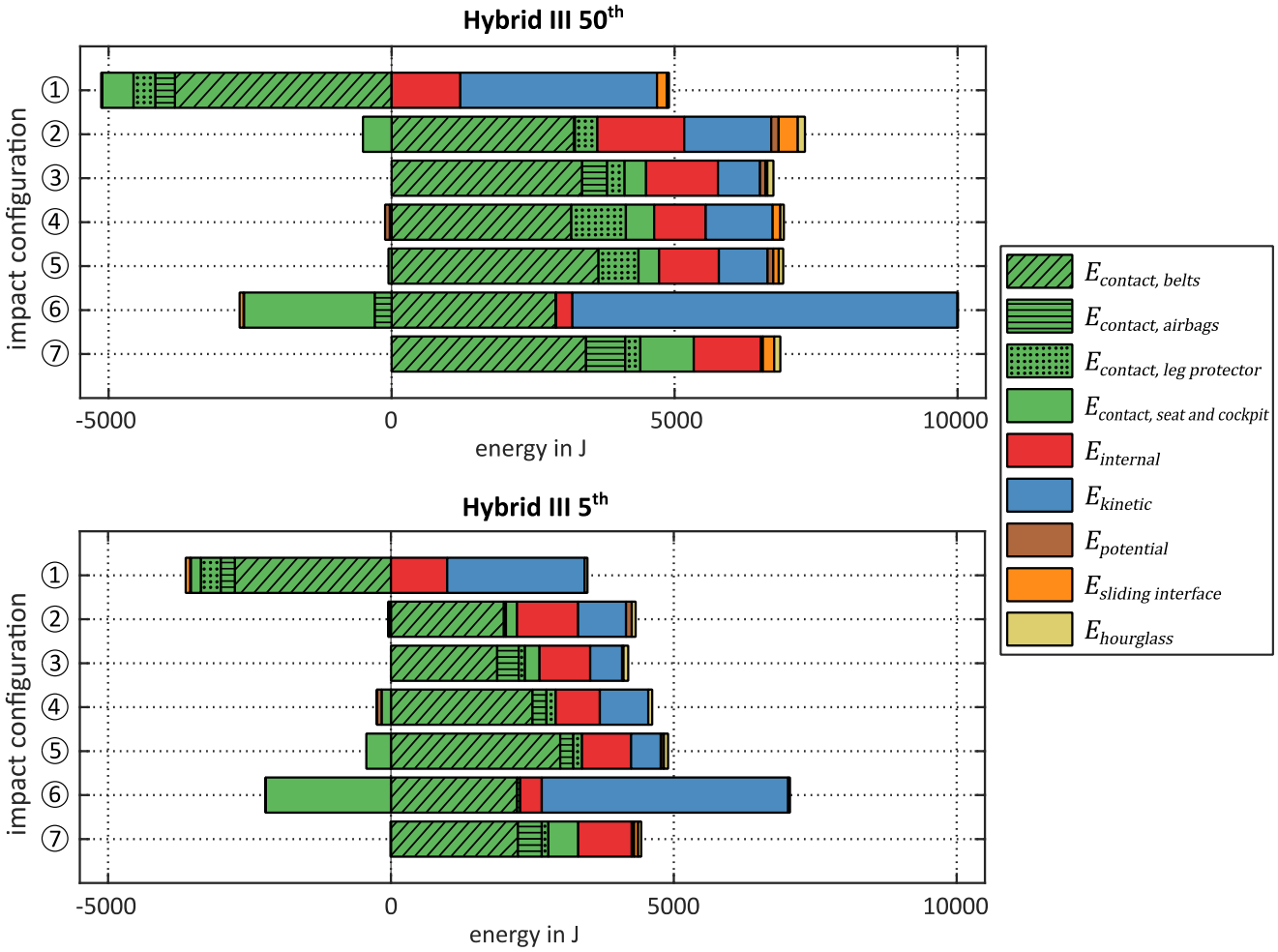

Fig. 12. Dummy energy balance in simulations' final state for all ISO 13232 impact configurations for 50th (top) and 5th (bottom) Hybrid III.

The overview of the configurations shows that they vary in the remaining kinetic energy, with high kinetic energy still remaining in accident configurations ① and ⑥. This means that these accident scenarios will have a secondary accident phase that should be considered. The very narrow bars of the potential energy represent the change in potential energy relative to the initial state. It shows that potential energy has no significant share in crash energy management for the primary impact. What also becomes clear is that in all scenarios with significant impact, which thus excludes scenario ⑥, some portion of internal energy is absorbed by the dummy. A ranking of the internal energies stored in the 5th and 50th dummy parts on the basis of an average for all impact scenarios, provided in Appendix D, shows that the majority was stored in the dummy's pelvis moulded foam, lumbar spine and rubber neck parts. For the 5th percentile dummy this also includes the shoulder pad part. This is followed by the larger outer moulding parts of the dummies. After all, the largest share is transmitted through the contacts.

Examining the contributors to the contact energies, the cumulative belt contact energy transfer in the final state always has the biggest share, comparatively. Depending on the configuration, the airbags and leg protectors have very different shares. There are still some significant energy portions that got transferred into the seat and other motorcycle cockpit surfaces. In configurations ⑦ and ③ the airbags decelerated the rider's significant upper-body rotation, as shown in Fig. 9. In accident configurations ④ and ⑤, with shallow impact angle and a more lateral motion of the rider, the airbags absorb less energy but the leg protectors absorb more energy. This is also shown in Fig. 9. The energy distribution in configuration ⑥ shows that the final state of energy transfers through belt vs. cockpit surfaces and seat almost completely counteract each other, with very low resultant contact energy transfer. This also means that the dummy overall kinetic energy is mostly conserved.

CORA Plus Objective Rating

To quantitively compare the dummy trajectory and acceleration data of the LS-DYNA FE simulations with the Madymo MB simulations for major dummy body parts, as shown in Fig. 13, the CORA (CORelation and Analysis) objective rating (version CORAplus Release 4.0.4) [15] was used. Here, the rating tool CORA offers an objective metric of the correlation of two-time history signals by combining two independent rating methods: a corridor rating and a cross-correlation rating. To consider multiple sensor signals for the relative displacement trajectories with channels for x-, y-, and z-directions vs. time, the parameter *MIN_NORM* was set to 1. This resulted in equal corridor widths and time intervals, which were determined for all axis channels based on the axis channel with the largest signal values. Apart from this, the default CORA metric parameters were used (see Table B.I in Appendix B for significant parameters). For the shown impact configuration ④, the displacement and acceleration data are provided in Appendix B, exemplary.

As shown in Fig. 14, the CORA metrics indicate an overall mostly excellent rating for the displacements and mostly at least fair rating for the resultant accelerations for head, thorax and pelvis. The acceleration signals of the FE dummy are, despite filtering, much noisier. In scenario ⑥ the accelerations do not agree well, due to generally very low loading in this impact configuration for the primary impact.

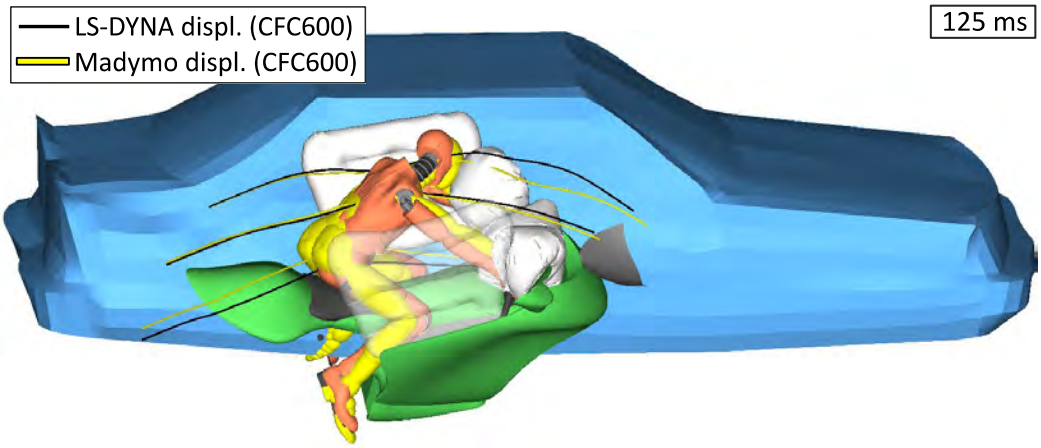

Fig. 13. Overlay of head, thorax and pelvis coordinate trajectories of ellipsoid MB dummy model in Madymo and FE dummy model in LS-DYNA simulation environment, shown here for impact configuration ④.

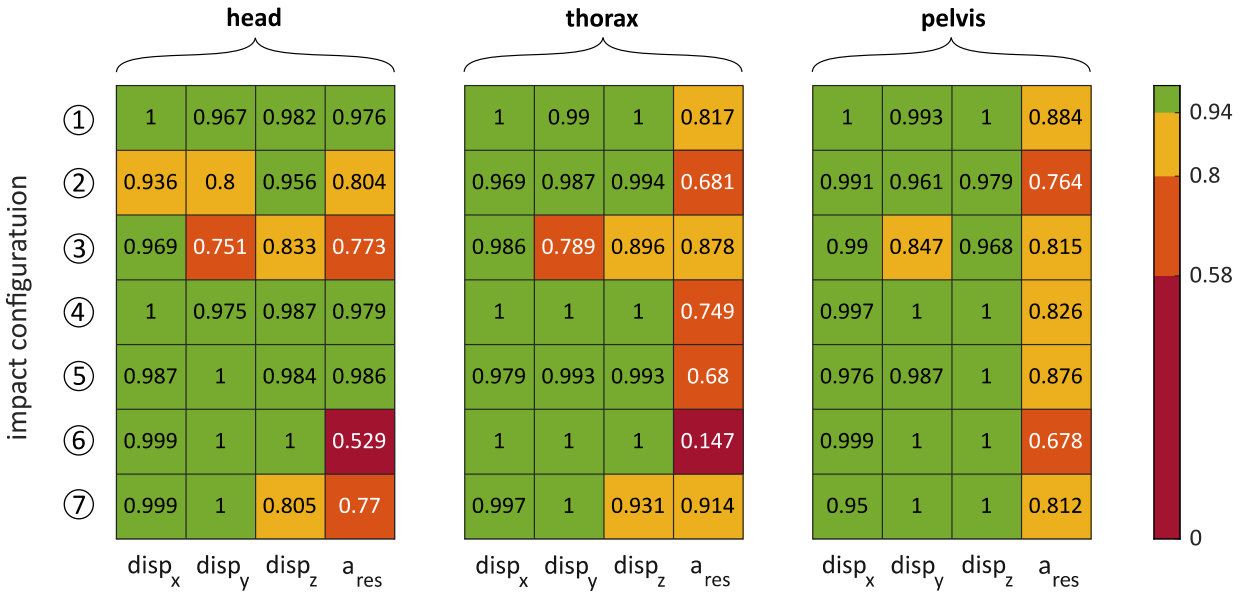

Fig. 14. CORA rating for dummy head, thorax and pelvis x-, y-, z-displacement and resultant acceleration of the Hybrid III 50th rider surrogate between Madymo and LS-DYNA environment. Categorized as excellent (>0.94), good (>0.8), fair (>0.58) and poor (<=) according to [16].

IV. Discussion

Compared to a chaotic and uncontrolled dismount, where the rider is exposed to the unpredictability of a motorcycle accident, in these accident configurations the riders showed predictable behaviour. This means that (i) restraining the rider to the motorcycle, (ii) decelerating the resulting upper body and lower body motions with airbags and leg impact protectors, and (iii) reducing the rider's interaction with the cockpit surfaces, e.g., the handlebars, led to a guided and controlled trajectory for the primary accident phase. This was shown for a small female and a mid-size male surrogate using the same passive safety design with identical system parameters. This also resulted in injury criteria for the vital body regions for the female and male rider within, and mostly well below, their respective biomechanical limits for all representative motorcycle accident scenarios according to ISO 13232. The safety system, designed for a single, non-helmeted rider, does not allow "hanging-off" the motorcycle while cornering because of the side-impact structure. However, the side impact structure and the energy absorbing foam proved effective in protecting the upper legs, despite the low profile of the impact protectors. In configurations with high belt forces, the belt force limitation resulted in belt elongation reducing the effective restraint of the rider in the subsequent accident phases. Combined with the potentially very complex nature of motorcycle accidents, especially after the first impact, and the variety of possible accident opponents, this presents major challenges for future studies on the design and assessment of protective measures in the subsequent accident phases.

The evaluation of the crash energy balances and the distribution of internally stored energy in the dummy parts for the simulations' final state provided further insight of the operation principles and possible injury mechanisms. Thus, potential injuries because of the large amount of internally stored energy in the deformable parts of the pelvis, due to the safety concept-related loading of the belts on a single body part, are not covered by corresponding injury criteria based on sensor data from the dummy. The energy balances also showed that there are scenarios, based on the chosen set of representative accident configurations, for which consideration of a subsequent secondary accident phase will be necessary.

Compared to the previously conducted combined MB and FE simulations in the earlier development steps, the simulations showed quantitatively very good agreement between the rider's accident trajectory and behaviour on the vehicle. This is crucial for a development process that successively incorporates previous results. The presented FE-model represents a much more detailed reproduction of the rider-motorcycle interaction. This includes: (i) a more accurate placement of the dummy's fingers around the handlebar grips; (ii) the implementation of a virtual characterization of a leg protector material to accurately represent absorption of the impact forces and dummy response; and (iii) more accurate contact methods for deformable objects, i.e., the dummy-to-motorcycle cockpit surface impacts.

To predict the impact behaviour of the motorcycle the underlying multi-body models of motorcycle and car were fitted based on comparisons of conventional motorcycles to full-scale crash tests in a previous study [11]. On this basis the model was used to replicate the impact of the motorcycle and the accident dynamics immediately after the first impact. Here, concept-specific conditions are advantageous. Compared to conventional motorcycle accidents where severe dummy to accident opponent contact is mostly imminent, here, direct dummy head and upper torso to car contact was avoided. Except for dummy to motorcycle body contact, all other dummy contacts were interactions of the dummy with compliant passive safety systems with higher degree of reliability and predictability, driven by more established automotive vehicle safety development. What the model cannot do is to reproduce the internal structure of the motorcycle, like the structural integrity of the side-impact structure and the structural response of deformable motorcycle outer body components. This currently necessitates the simplification of not considering contacts between the dummy legs and the accident opponent, which currently potentially underestimates leg injuries caused by contact with the accident opponent. Therefore, the model was also not used to analyse the behaviour in more complex subsequent accident phases and/or in interaction with other objects like roadside barriers. To eventually reproduce the internal structure and further representative accident configurations in the future, a further detailing step in the modelling of the motorcycle and the accident opponent in a FE environment combined with further validation procedures will be necessary. The dummy type used was developed specifically for frontal impacts. However, a dummy type that is more suitable for the given application does currently not exist. In the future, human body models can be used here, at least in the virtual environment.

V. CONCLUSIONS

Simulations of recommended ISO 13232 accident configurations of a novel safety concept that restrains a non-helmeted motorcyclist to the motorcycle showed promising performance in the primary accident phase for female and male rider surrogates. Similar to safety systems for car occupants, a combination of several passive safety systems has shown effective to control and guide the motorcyclist's accident trajectory. A simulation methodology, as part of a multi-stage development process with successive increases in complexity and expected fidelity, allowed detailed representation of diverse motorcyclists and their interaction with a motorcycle and its passive safety equipment while efficiently incorporating full vehicle interaction. The model and simulation methodology are not able to represent deformations of the outer motorcycle geometry and was therefore not used to predict the motorcycle's behaviour in more complex subsequent accident phases and/or in interaction with other roadside objects. Assessing detrimental effects of the rider being belted to the motorcycle in these phases will especially crucial since the rider is intended to be non-helmeted and without further safety clothing.

VI. ACKNOWLEDGEMENT

This work is funded by the State Ministry of Baden-Württemberg for Economic Affairs, Labour and Housing Construction within the programme of Innovative Mobility Solutions and supported by the Stuttgart Center for Simulation Science (SimTech).

VII. REFERENCES

[1] European Commission (2018) Power Two Wheelers. European Commission, Directorate General for Transport, 2018.

[2] Statistisches Bundesamt (2019) Verkehr: Verkehrsunfälle. *Verkehr*, **8**(7): 2019.

[3] Kraftfahrtbundesamt "Verkehr in Kilometern - Inländerfahrleistung". https://www.kba.de/DE/Statistik/Kraftverkehr/VerkehrKilometer/vk_inlaenderfahrleistung/vk_inlaenderfahrleistung_inhalt.html. [2021-08-03]

[4] Piantini, S., Pierini, M., *et al.* (2016) Injury Analysis of Powered Two-Wheeler versus Other-Vehicle Urban Accidents. *Proceedings of IRCOBI Conference*, 2016, Malaga, Spain.

[5] Amadesi, A., Cerutti, E., *et al.* (2016) The Toll of Traffic-Related Fatalities in a Metropolitan Italian Area Through the Experience of the Department of Legal Medicine. *International Journal of Injury Control and Safety Promotion*, **23**(2): pp.197–205.

[6] Berg, F. A., Rücker, P., *et al.* (2011) Bundesanstalt für Straßenwesen. *Prüfverfahren für die passive Sicherheit motorisierter Zweiräder*, Bergisch Gladbach, Germany.

[7] Kuroe, T., Namiki, H., Iijima, S. (2005) Exploratory study of an airbag concept for a large touring motorcycle: Further research second report. *19th International Technical Conference on the Enhanced Safety of Vehicles,* 2005, Washington DC, United States.

[8] Kalliske, I., Albus, C., Faerber, E. (1998) Bundesanstalt für Straßenwesen. *Beurteilung der Sicherheitsaspekte eines neuartigen Zweiradkonzeptes*, Bergisch Gladbach, Germany.

[9] Grassi, A., Barbani, D., Baldanzini, N., Barbieri, R., Pierini, M. (2018) Belted Safety Jacket: A New Concept in Powered Two-Wheeler Passive Safety, *Procedia Structural Integrity,* 2018, **8**:pp.573–593.

[10] Murri, R. (2007) Sicherheitsgurt für Motorräder - Lösungsansätze, Schutzpotenzial und Crashergebnisse. *Verkehrsunfall und Fahrzeugtechnik*, 2007, **45**(12):pp.341–344.

[11] Maier, S., Doléac, L., Hertneck, H., Stahlschmidt, S., Fehr, J. (2020) Evaluation of a Novel Passive Safety Concept for Motorcycles with Combined Multi-Body and Finite Element Simulations. *Proceedings of IRCOBI Conference*, 2020, Munich, Germany.

[12] ISO 13232:2005 (2005) Motorcycles – Test and analysis procedures for research evaluation of rider crash protective devices fitted to motorcycles.

[13] Livermore Software Technology Corporation (2016) LS-DYNA Keyword User's Manual Volume II Material Models LS-DYNA R9.0, 2016, Livermore, USA.

[14] Eppinger, R., Sun, E., *et al.* (1999) *Development of Improved Injury Criteria for the Assessment of Advanced Automotive Restraint Systems – II.* National Highway Traffic Safety Administration, Washington DC, USA.

[15] Gehre, C., Gades, H., Wernicke, P. (2009) Objective Rating of Signals Using Test and Simulation Responses. *Proceedings of the 21st International Technical Conference on Experimental Safety Vehicles (ESV),* 2009, Stuttgart, Germany.

[16] Thunert, C. (2017) CORAplus Release 4.0.4 User's Manual, 2017.

VIII. APPENDICES

Appendix A: Bipolynomial Regression of Dynamic and Quasi-Static Experimental Data

The stress data points (z) of the dynamic measurements shown in Fig. 3 up to the maximum stress were fitted using bipolynomial regression on a rectilinear 2D grid for strain (x) and strain rate (y) with coefficients $\boldsymbol{b}$ and $\boldsymbol{c}$.

$$z = F(x,y) = (b_0 + b_1 x + b_2 x^2 + \cdots + b_n x^n) \cdot (c_0 + c_1 y + c_2 y^2 + \cdots + c_m y^m) \tag{1}$$

with polynomial degree n for the strain (x) and m for the strain rate (y). Computing and renaming the grouped factors e.g., for $n = 1, m = 2$ leads to:

$$F(x,y) = a_0 + a_1 x + a_2 y + a_3 xy + a_4 y^2 + a_5 xy^2, \tag{2}$$

where the polynomial coefficients $\boldsymbol{a}$ approximate all k-data points

$$\underbrace{\begin{bmatrix} z_1 \\ z_2 \\ \vdots \\ z_k \end{bmatrix}}_{\boldsymbol{b}} \approx \underbrace{\begin{bmatrix} 1 & x_1 & y_1 & x_1 y_1 & y_1^2 & x_1 y_1^2 \\ 1 & x_2 & y_2 & x_2 y_2 & y_2^2 & x_2 y_2^2 \\ \vdots & \vdots & \vdots & \vdots & \vdots & \vdots \\ 1 & x_k & y_k & x_k y_k & y_k^2 & x_k y_k^2 \end{bmatrix}}_{\boldsymbol{A}} \cdot \underbrace{\begin{bmatrix} a_1 \\ a_2 \\ a_3 \\ a_4 \\ a_5 \end{bmatrix}}_{\boldsymbol{a}}. \tag{3}$$

The coefficients were determined through minimization of a quadratic objective function, with linear equality and inequality constraints incorporating LS-DYNA material card requirements and knowledge about surface topology to sustain a physically valid shape in surface regions with sparse or no data:

$$\min_{\boldsymbol{a}} \|\boldsymbol{b} - \boldsymbol{A}\boldsymbol{a}\|_2 \text{ such that } \begin{cases} F(0,y) = 0 \text{ : ensure strain rate-axis intersection} \\ \frac{\partial}{\partial x} F(x) > 0, \\ \frac{\partial}{\partial y} F(y) > 0 \text{ : curves must not intersect and increase in strain direction} \\ \frac{\partial}{\partial y} F(y) \leq p_1 \text{ : limit slope } p_1 \text{ in strain rate direction} \\ \frac{\partial^2}{\partial x^2} F(x) > 0 \text{ for } x > p_2 \cdot x_{max} \text{ with } p_2 \epsilon [0\,,1] \text{: positive curvature in an upper portion } p_2 \text{ up to maximal strain } x_{max} \text{ in strain direction} \end{cases} \tag{4}$$

In addition to the introduced parameters p_1 and p_2 to control the surface fit, a parameter p_3 was introduced to describe a logarithmic order of the non-uniformly spaced 2D grid in strain direction. This shifts a finer discretization to lower or higher strains where the matched surface's curvature might be higher and reduces the required polynomial order for an adequate fit. The ultimately desired curves of constant velocities for the material card are sections of the created surface, seen in Fig. 5. The unloading data of the quasi-static measurements were fitted with the same procedure, but with $m = 0$.

Appendix B: Cora Plus Rating Parameters and Exemplary Comparison for Impact Configuration ⑦ (414-6.7/13.4)

TABLE B.I
CORAPLUS RATING PARAMETERS USED IN THIS STUDY

transition exponent	rating exponents			cross correlation weights			method weights	
K	K_V	K_G	K_P	G_V	G_G	G_P	G_1	G_2
2	10	1	1	0.333	0.333	0.333	0.5	0.5

phase limits		minimum time interval
D_{MIN}	D_{MAX}	INT_{MIN}
0.01	0.12	0.8

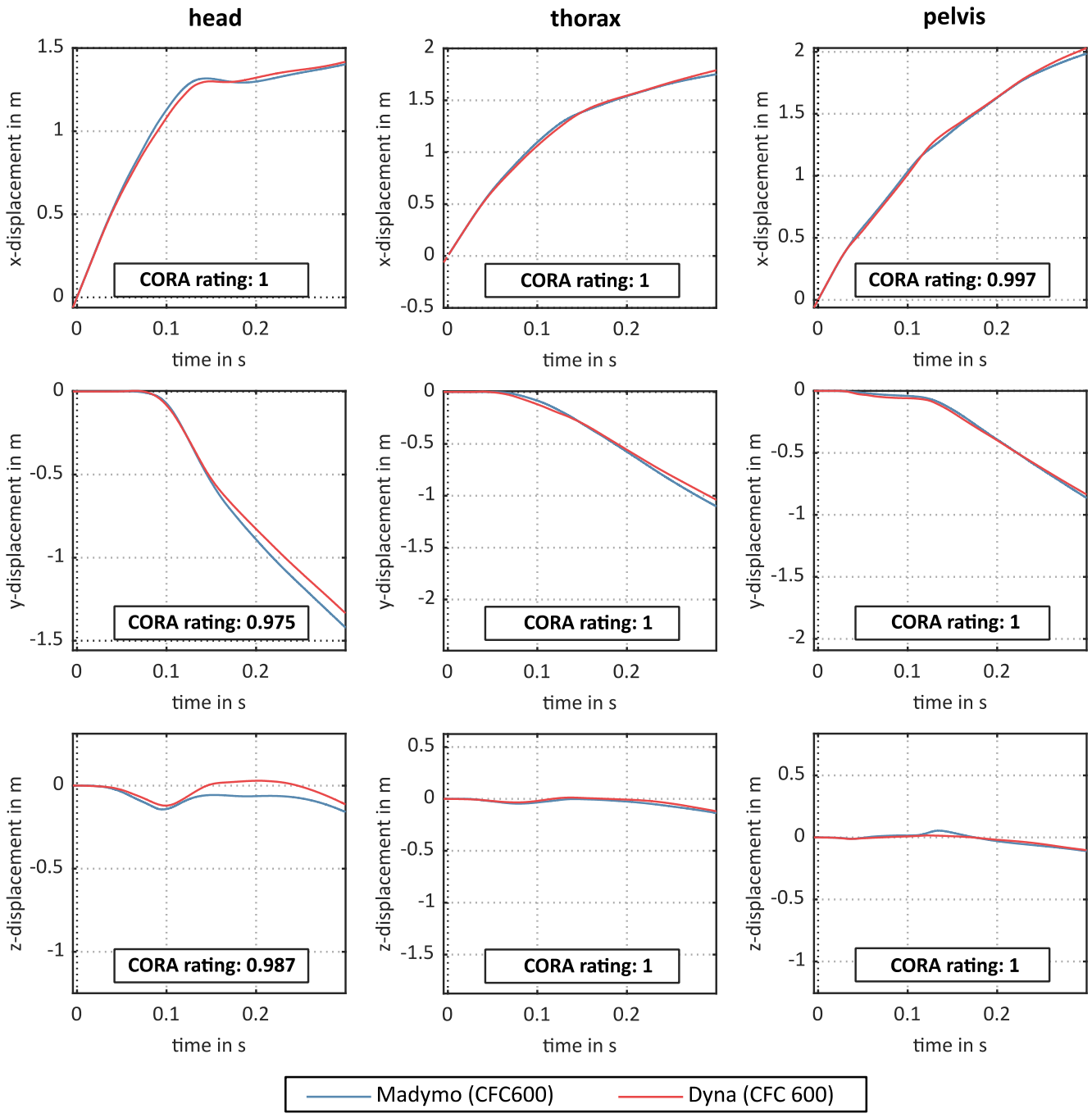

Fig. B1. Comparison of dummy head, thorax and pelvis x-, y-, z-displacement of Hybrid III 50th rider surrogate in configuration ④ between Madymo and LS-DYNA environment with CORA ratings.

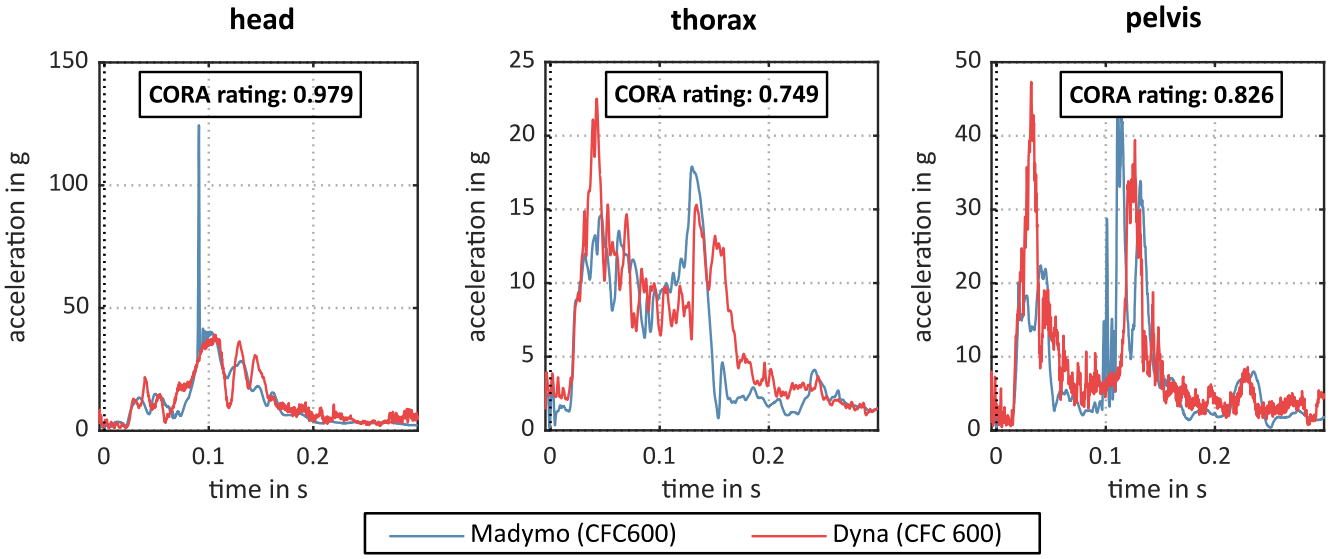

Fig. B2. Comparison of dummy head, thorax and pelvis resultant accelerations of Hybrid III 50th rider surrogate in configuration ④ between Madymo and LS-DYNA environment with CORA ratings.

Appendix C: Injury Criteria and Biomechanical Limits

TABLE C.I
EVALUATED INJURY CRITERIA WITH RESPECTIVE BIOMECHANICAL LIMITS [6][14]

body region	criterion	abbreviation	limit
head	head Injury Criterion (36 ms)	HIC(36)	1000
	resultant head acceleration	a_{3ms}	80 g over 3 ms
neck	neck tensile force	$F_{z,\,tens,\,1ms}$	3.3 kN over 1 ms
		$F_{z,\,tens,\,45ms}$	1.1 kN over 45 ms
	neck compression force	$F_{z,\,compr,\,1ms}$	4 kN over 1 ms
		$F_{z,\,compr,\,45ms}$	1.1 kN over 45 ms
	neck shear forces	$F_{xy,\,1ms}$	3.1 kN over 45 ms
		$F_{xy,\,45ms}$	1.1 kN over 45 ms
	neck rearward moment	$M_{y,\,fwd,\,max}$	57 Nm
	neck forward moment	$M_{y,\,rwd,\,max}$	190 Nm
	neck injury criterion	NIJ_{max}	1
thorax	resultant thorax acceleration	a_{3ms}	60 g over 3 ms
	chest deflection	$Defl_{max}$	75 mm
pelvis	resultant pelvis acceleration	a_{3ms}	60 g over 3 ms
femur	femur axial force	$\lvert F_z \rvert_{max}$	10 kN
tibia	tibia index	TI	1.3

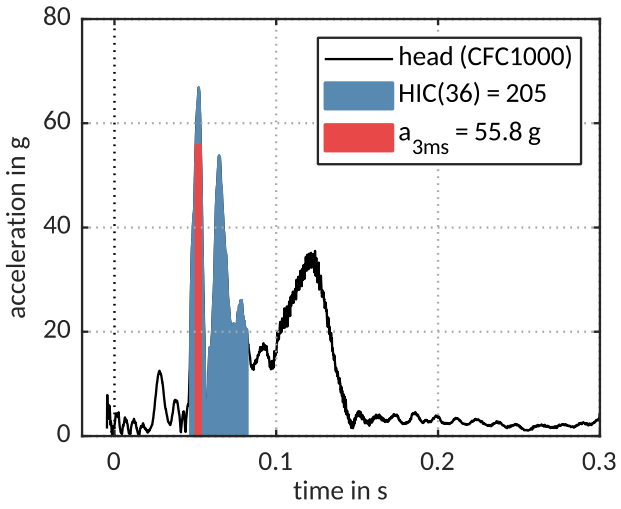

Fig. C1. Head linear acceleration for configuration ⑦.

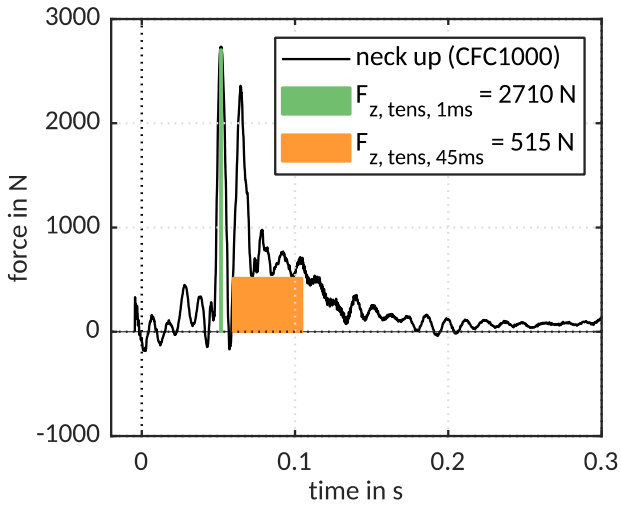

Fig. C2. Neck tensile force for configuration ⑦.

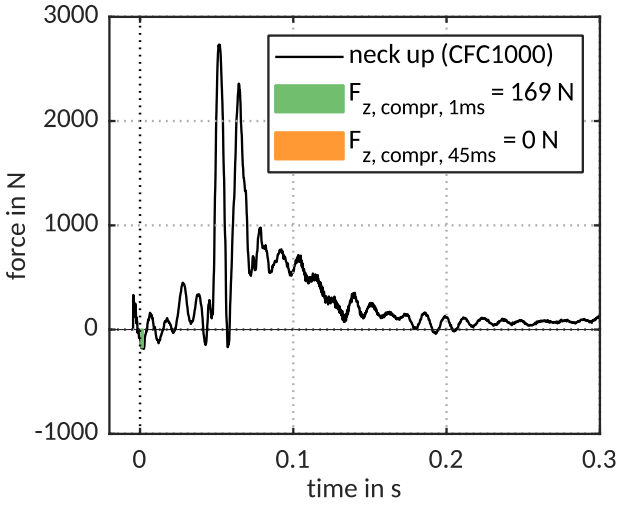

Fig. C3. Neck compression force for configuration ⑦.

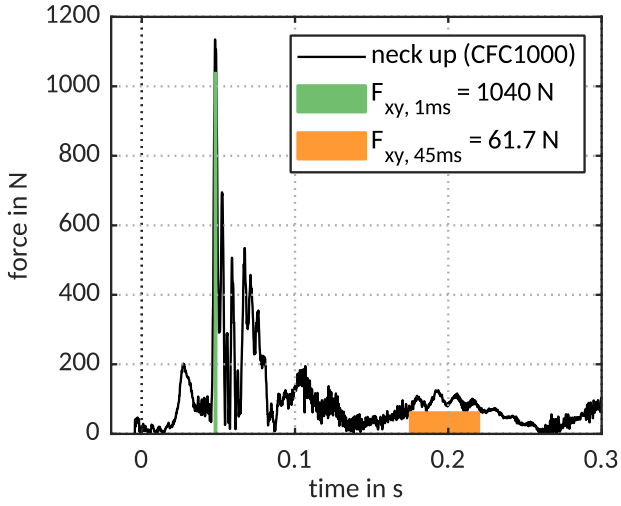

Fig. C4. Neck shear forces for configuration ⑦.

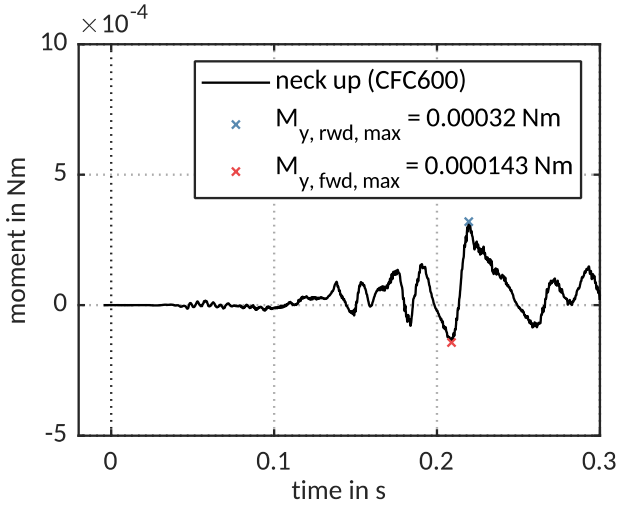

Fig. C5. Neck flexion and extension moment for configuration ⑦.

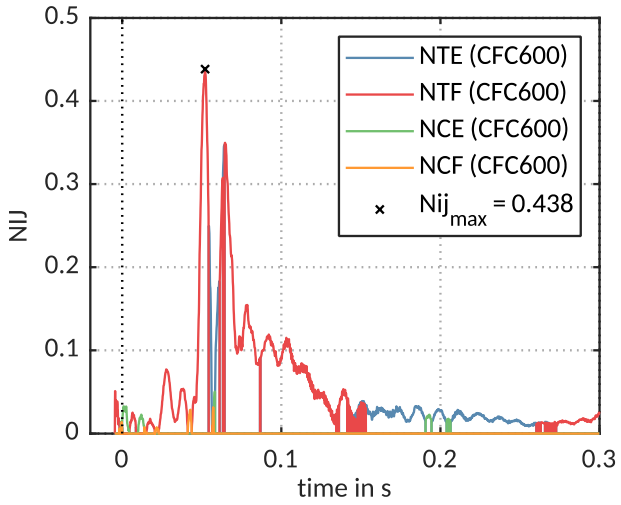

Fig. C6. Neck injury criterion for configuration ⑦.

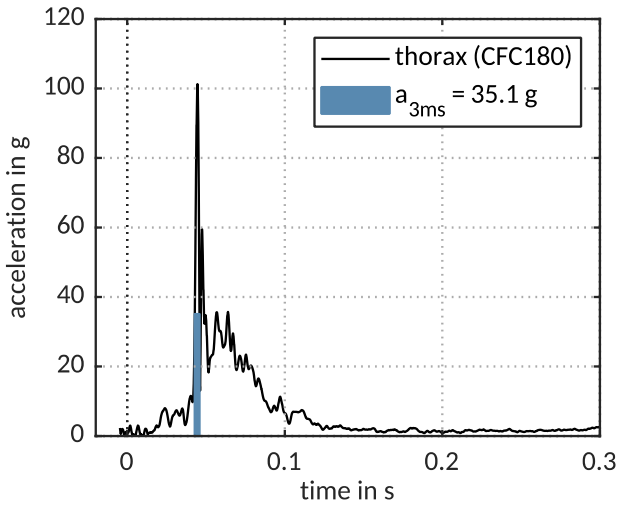

Fig. C7. Thorax linear acceleration for configuration ⑦.

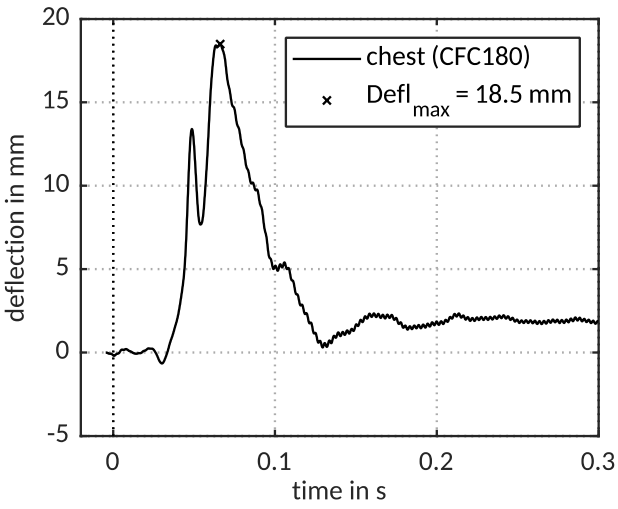

Fig. C8. Chest deflection for configuration ⑦.

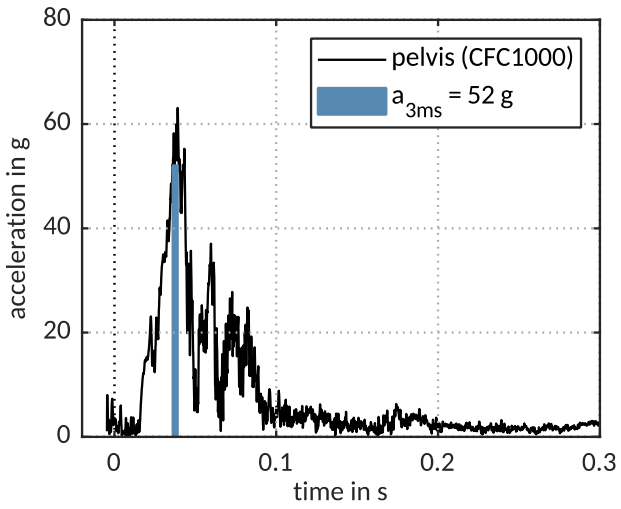

Fig. C9. Pelvis linear acceleration for configuration ⑦.

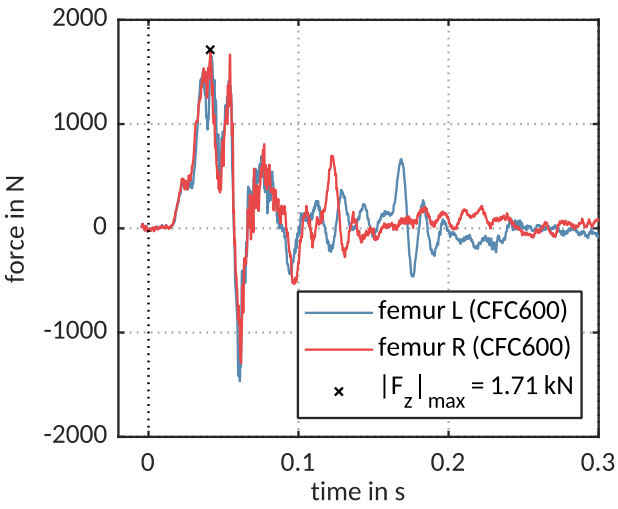

Fig. C10. Femur axial forces for configuration ⑦.

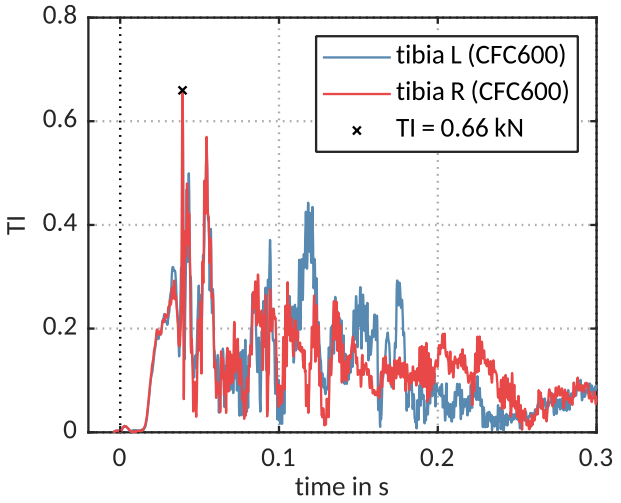

Fig. C11. Tibia index for configuration ⑦.

Appendix D: Internally Stored Energy in Dummy Parts

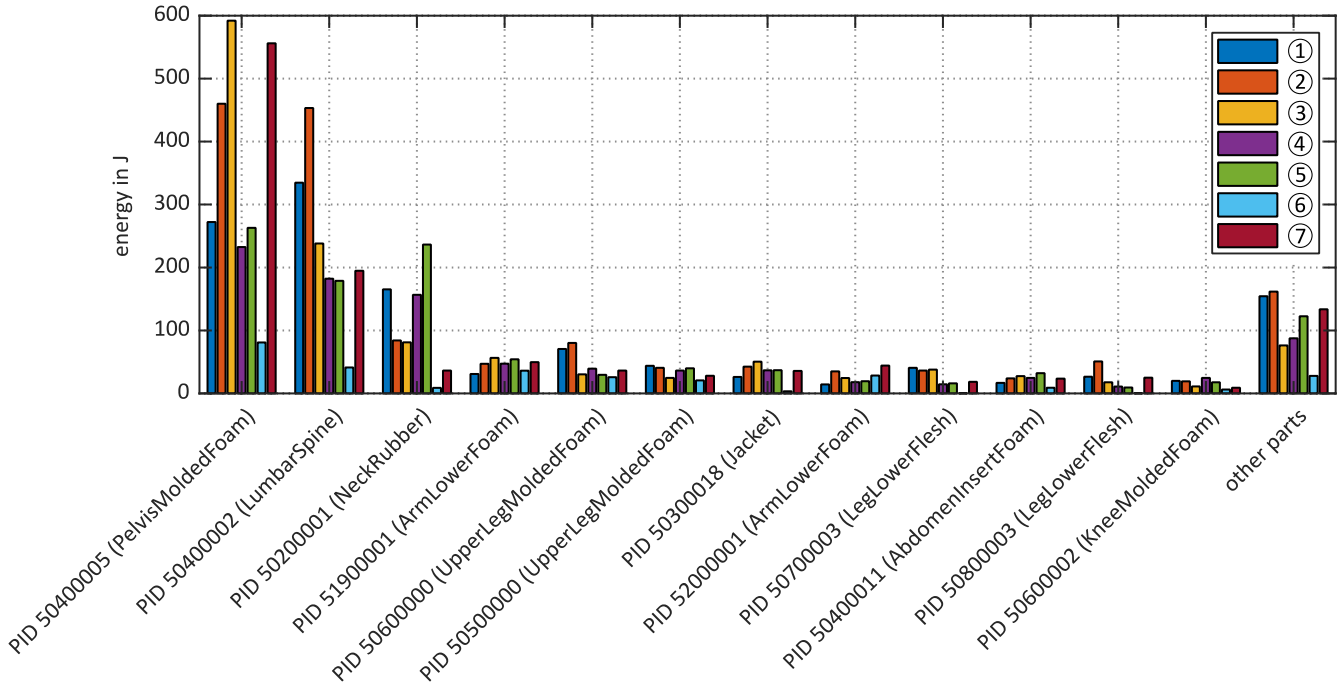

Fig. D1. Internal energies stored in the Hybrid III 50th dummy parts, ranked by the average internal energy for all impact configurations ① to ⑦.

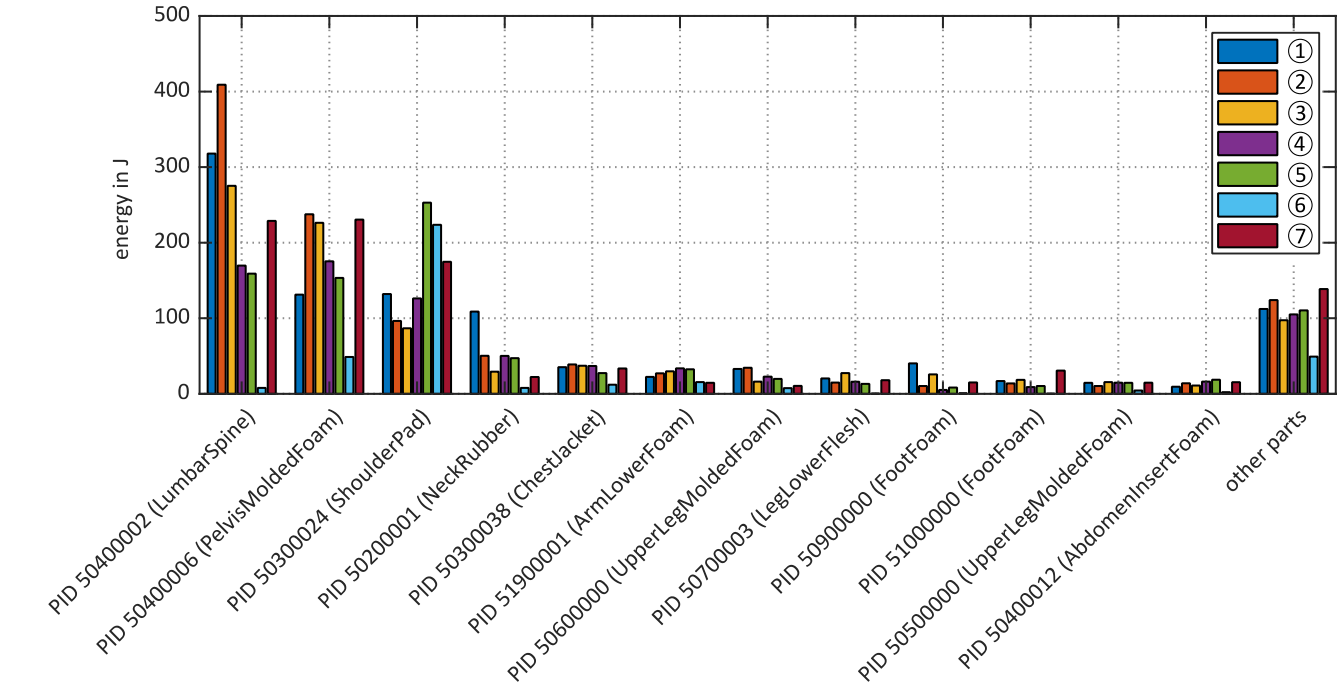

Fig. D2. Internal energies stored in the Hybrid III 5th dummy parts, ranked by the average internal energy for all impact configurations ① to ⑦.